REVISION 2

Formation of rhyolite at the Okataina Volcanic Complex, New Zealand: New insights from analysis of quartz clusters in plutonic lithics

Karina A. Graeter[1], Rachel J. Beane[1], Chad D. Deering[2], Darren Gravley[3], and Olivier Bachmann[4]

[1] Department of Earth and Oceanographic Science, Bowdoin College, Brunswick, Maine 04011, U.S.A.

[2]Department of Geological and Mining Engineering Sciences, Michigan Technological University, Houghton, Michigan 49931, U.S.A.

[3]Department of Geology, University of Canterbury, Christchurch, New Zealand 8140

[4] Institute of Geochemistry and Petrology, ETH Zurich, NW Clausiusstrasse 25, 8092 Zurich, Switzerland

ABSTRACT

Granitoid lithic clasts from the 0.7 ka Kaharoa eruption at the Tarawera volcano (Okataina Volcanic Complex, Taupo Volcanic Zone, New Zealand) provide insight into the processes of rhyolite formation. The plutonic lithic clasts of the Kaharoa eruption consist of (1) quartz phenocrysts, which are often grouped into clusters of two to eight quartz grains, (2) plagioclase phenocrysts (mostly ~An_{40} with up to An_{60} cores), and (3) interstitial alkali feldspar. Quartz orientations obtained through electron backscatter diffraction (EBSD) methods show that 78% of the 82 analyzed clusters have at least one pair of quartz grains with the dominant dipyramidal faces matched. Variations in cathodoluminescence (CL) zoning patterns of the quartz suggest that quartz clusters came together after initial crystal growth and that many quartz

crystals were subject to one or more resorption events. The process of quartz crystals with different magmatic histories coming together into common relative orientations to form clusters is indicative of oriented quartz synneusis and suggests a history of crystal accumulation. The quartz clusters are interpreted to have formed as part of a crystal cumulate mush within a shallow magma chamber where quartz crystals rotated into contact along their dominant dipyramidal faces during hindered settling and/or compaction. The preservation of oriented quartz clusters from the Kaharoa plutonic lithics thus provides evidence for synchronous, shallow pluton formation from a cumulate mush during active silicic volcanism. This result is consistent with models whereby melt-rich, high-silica rhyolite formation occurs via interstitial melt extraction from a low-silica rhyolite mush in the shallow crust.

Keywords: Cathodoluminescence, Cumulate, EBSD, Rhyolite Formation, Taupo Volcanic Zone

INTRODUCTION

In young, rhyolite generating regions such as the central Taupo Volcanic zone (TVZ), any potential plutonic portions of the magma system have not been exposed by uplift or erosion. Without exposure of the plutonic portions, the connection between volcanic and plutonic processes remains uncertain, with multiple models proposed for rhyolite formation. Towards one end of the spectrum of models, eruptible felsic magma forms slowly at shallow depths through the processes of crystal fractionation and interstitial melt extraction from an incrementally-built intermediate crystal mush, which is preserved as a cumulate in the rock record (c.f., Bachmann and Bergantz, 2004; Hildreth and Wilson, 2007; Deering and Bachmann, 2010). Towards the other end of the spectrum, plutonic and volcanic systems are only distantly related, with eruptible felsic magma generated at greater depths and residing transiently in the shallow crust (c.f.,

Coleman et al. 2012; Tappa et al., 2011; Glazner et al., 2004; Bartley et al., 2008). For some of these models, felsic plutons are also emplaced incrementally in the shallow crust and cool to the solidus in between all new recharge without further differentiation in the upper crust. Hence, the plutonic left-overs are largely unrelated to the waxing stage of the system when melt-rich magma is erupted (Glazner et al., 2004).

To address differences in the models, coeval silicic plutonic and volcanic units should be directly compared. In the TVZ and other young volcanic regions, fully crystalline lithologies are confined to plutonic lithics – exhumed fragments of holocrystalline rock that solidified before or concurrent with eruption. The source of the plutonic fragments is the magma reservoir in which the magma resides prior to eruption. Plutonic lithics obviously reflect high degrees of crystallization and imply that, in active volcanic complexes, at least some portions of the magma reservoir reach the solidus. Therefore, these lithics can help better connect the plutonic and volcanic processes.

Interpretation of plutonic lithics requires care as they may originate from different stages of the magmatic evolution of a volcano: (1) magma crystallized along the carapace during previous episodes of eruption (Charlier et al., 2003; Bacon and Lowenstern, 2005, Bachmann, 2010), (2) an earlier solidified or chemically distinct injection of magma into the shallow crust that is unrelated to active rhyolite formation (Keller, 1969; Lowenstern et al., 2000; Charlier et al., 2003; Vazquez et al., 2007), or (3) a solidified portion of a cumulate crystal mush (Burt et al., 1998). Thus, we first establish the origin and timing of formation of the TVZ plutonic lithics before using them to interpret the magma chamber processes.

We examine granitoid plutonic lithics exhumed during the 0.7 ka Kaharoa eruption event at the Okataina Volcanic Complex (OVC; Fig. 1). These granitoid plutonic lithics are geochemically (major and trace elements, radiogenic and stable isotopes) similar to the Kaharoa and other OVC rhyolite magmas (Brown et al., 1998). Zircon dating suggests that the Kaharoa plutonic lithics completed crystallizing zircon (i.e. reached the solidus) around 125 ka (Shane et al., 2012), compared to a range between 200 ka to 0.7 ka for zircon in the Kaharoa rhyolite (weighted average model ages; Klemetti et al., 2011; Storm et al. 2012). Thus, while the initial parent magma for both the rhyolite and plutonic magmas may have been the same, it is likely that the evolution of the two bodies was temporally distinct. Both the Kaharoa rhyolite and the lithics exhumed with them were derived from shallow levels within the crust at pressures c. 100 MPa (c.f. Bryan et al., 1999; Deering et al., 2012; Shane et al., 2012; Bégué et al., 2014).

When combined, the previous research suggests that the Kaharoa plutonic lithics came from the shallow portion of the magma system, and were not interacting with the rhyolite magma immediately prior to the Kaharoa event. The origin of the Kaharoa plutonic lithics and their potential relationship to the high-silica rhyolite of the OVC remains unclear; Previous interpretations suggested the plutonic lithics are (1) pieces from the carapace of the magma system (Deering et al., 2012), or (2) an isolated magma injection into the shallow crust (Shane et al., 2012). Another possible origin of the plutonic lithics is a crystal mush that formed via crystal fractionation in the shallow crust, resulting in the production of high-silica rhyolite commonly erupted at the OVC.

To distinguish between these possibilities, we analyze quartz clusters in the Kaharoa plutonic lithics. Previous research used electron backscatter diffraction (EBSD) and

Cathodoluminescence (CL) imaging methods to interpret magma evolution from quartz clusters (Wiebe et al., 2007; Beane and Wiebe 2012). Our analysis of quartz clusters allows us to interpret the origin of the Kaharoa plutonic lithics and document the processes occurring below the Okataina Volcanic Complex.

GEOLOGIC SETTING

Magmatism of the Taupo Volcanic Zone (TVZ), New Zealand, has produced more than 10,000 km^3 of volcanic deposits from the late Pleistocene to present (Wilson et al., 1995). Eight rhyolite calderas dominate the central TVZ with activity in the past ~60 kyr focused at two volcanic centers: Taupo and Okataina (Deering et al., 2012 and references therein; Wilson et al., 2009). The Okataina Volcanic Complex (OVC; Fig. 1) has been one of the most active and productive calderas in recent history (Wilson et al., 1995; Wilson et al., 2009). In addition, intra-caldera volcanism within the OVC has occurred at the Tarawera Volcano and the Haroharo Volcano within the OVC (Nairn et al., 2004). At Tarawera, four rhyolitic eruptions at 21.9 ka, 17.7 ka, 13.7 ka, and 0.7 ka have occurred with the youngest being the Kaharoa eruption (Shane et al., 2008; Shane et al., 2012).

Nairn et al. (2001 and 2004) detailed the sequence of events that occurred during, and just prior to, the Kaharoa eruption at 0.7 ka. The event was initiated by repeated injections of basaltic magma into a high-silica rhyolite (comagmatic basaltic enclaves are found throughout the volcanic sequence). Approximately 4 km^3 of magma was erupted from seven vents. The Kaharoa eruptive deposits consist primarily of rhyolite pumice, ash, lapilli, and blocks. These are accompanied by common accessory lithic clasts from earlier Tarawera rhyolite lavas, clasts from

the intruding basalt, and rare plutonic lithic clasts. The Kaharoa eruptive episode ended with block-and-ash flow deposits and the extrusion of three lava domes.

METHODS

Sample Descriptions

Plutonic lithic fragments were collected from the re-worked deposits in gullies that cut the Kaharoa eruptive deposits southeast of the Tarawera dome (Leonard et al., 2002). Thirteen thin sections were made from two samples, five from sample KaLi4A and eight from sample KaLi102A. Samples are highly friable, and as a result some quartz grains were plucked during the polishing process. Grain pairs were identified within each cluster using petrography and cathodoluminescence imaging.

Analytical Methods

Thin sections of samples were analyzed using automated scanning electron microscopy (QEMSCAN) at the Colorado School of Mines to determine the mineral modes and approximate compositions. The carbon coated thin sections were loaded into the QEMSCAN instrument and the analyses were initiated using the control program (iDiscover, FEI). Four energy dispersive X-ray (EDX) spectrometers acquired spectra with a beam stepping interval (i.e., spacing between acquisition points) of 20μm, an accelerating voltage of 25 keV, and a beam current of 5 nA. The collected EDX spectra were compared with spectra held in a look-up table to assign a composition to each acquisition point and create a compositional map. Note that the assignment makes no distinction between mineral species and amorphous grains of similar composition. Results were output by the QEMSCAN software as a spreadsheet giving the volume percent (volume %) of each composition in the look-up table.

Cathodoluminescence (CL) images were obtained from three samples at the University of Canterbury, Christchurch, New Zealand and from eight samples at the Swiss Federal Institute of Technology in Zurich (*ETHZ*). The CL emission intensity in igneous quartz depends on Ti concentration (Wark and Spear, 2005). In turn, the concentration of Ti in igneous quartz correlates with the temperature of crystallization (Wark and Watson, 2006). Thus, CL imaging of quartz grains illuminates changes in the crystallization environment as well as brittle and ductile deformation features (Fig 2I). Images were taken of 170 quartz grain pairs that were identified using a petrographic microscope. At the University of Canterbury, carbon coated samples were imaged with a Gatan MiniCL attached to a JEOL 700f Scanning Electron Microscope (SEM) using an accelerating voltage of 15 kV and a beam current of between 15 and 20 nA. At ETHZ, carbon coated samples were imaged using a Gatan MiniCL attached to a FEI Quanta 200 FEG SEM using an accelerating voltage of 20 kV and a beam current between 15 and 20 nA.

Electron backscatter diffraction (EBSD) methods measure the diffraction patterns (Kikuchi bands) that form as electrons escape from the sample along different lattice planes. To index the diffraction patterns, the measured EBSD patterns are compared to patterns modeled from known lattice parameters using a kinematic electron diffraction model (Schmidt and Olesen, 1989, Prior et al., 1999). These indices produce 3-D crystallographic orientation data.

Electron backscatter diffraction (EBSD) patterns were collected from 187 quartz grain pairs in 13 samples at Bowdoin College using an HKL Nordlys II detector on a LEO 1450VP SEM and Channel5 software. Sample preparation included ~three hours of polishing in a noncrystallizing colloidal silica suspension on a Bueler Vibromet2 vibratory polisher (SYTON method of Fynn and Powel, 1979). Samples were not carbon coated; charging of the samples was

minimized by tilting the sample 70° and maintaining the chamber at a pressure of 15 Pa. The EBSD patterns were obtained using an accelerating voltage of 20 kV, beam current of 2.2 nA, and a working distance of 25 mm. Channel5 acquisition and indexing settings were 4x4 binning, high gain, Hough resolution = 80, 7 bands, 80 reflectors and 20 μm step size for orientation maps. Quartz was indexed using the lattice parameters of Sands (1969). The relative precision of the data are approximately 1º based on the number of bands (7) detected combined with the experimental work of Krieger-Lassen (1995) on the precision of crystal orientation measurements. After indexing, the 3-D crystallographic data for adjoining grains within clusters were plotted on upper hemisphere stereographic projections (Fig. 2). For each pair of grains, the angles between the c-axes and the angles between the poles to the dipyramidal faces were measured (Supplementary Material).

RESULTS

QEMSCANS and Petrography

In general, the QEMSCANs from both samples corroborate previous descriptions of the lithics' mineral composition and modes (Fig. 3 and Fig. 4; see Nairn et al., 2004), but provide a much improved modal analysis and characterization of the relationship between texture and mineral composition. Plagioclase forms primarily as phenocrysts, whereas quartz occurs as both large phenocrysts and interstitial crystals. Plagioclase phenocrysts are dominantly An_{20-40} with small An_{40-60}cores (Fig.4). Optically, all plagioclase grains exhibit extensive twinning and most show a varying degree of oscillatory zoning. Alkali feldspar is only interstitial. Quartz phenocrysts are highly fractured, resulting in phenocrysts that either appear equant with smooth grain boundaries or fragmented with jagged grain boundaries Alkali feldspar, later stage quartz,

and possibly low-Ca plagioclase (~albite) have filled in cracks and holes of many quartz phenocrysts. Biotite is present as relatively small (~0.05 mm to < 1.5 mm) dispersed flakes, associated with Fe-Ti oxides and hornblende, and with occasional inclusions of quartz and alkali feldspar.

CL Imaging

Cathodoluminescence images were acquired for 170 grain pairs (Fig. 5). To determine whether grains within quartz pairs had contrasting growth histories, we compared the pattern of the CL emission intensity zones and looked for unique resorption features in each grain. We avoided making interpretations based on pattern differences that could arise from the two-dimensional slicing of three-dimensional crystals, such as an apparent core in one grain and not in another. Major non-periodic discontinuities in zoning (50-1000 μm) are the result of changes in external factors such as temperature, pressure, and magma composition, while fine oscillatory zoning (2-20 μm) within these broader zones is the result of a diffusion-controlled mechanism on the crystal-melt boundary layer (Müller, 2000 and references therein)

We determined that most crystals within quartz grain pairs have dissimilar growth histories (see fig 5c,d, and e). For 12 grain pairs, zoning was too faint to confidently determine separate growth histories, and 17 grain pairs were not imaged. No images suggest that any pairs are fragments of larger phenocrysts. Sometimes, CL images revealed that supposed large quartz phenocrysts were actually made up of two or more individually zoned smaller phenocrysts (e.g. Fig 5c and e). Thus, CL imaging resulted in the detection of ~50 additional grain pairs that were not initially observed with the petrographic microscope because they were in the same orientation (had the same extinction angle).

Evidence of resorption is observable in ~32 grains. There are irregular resorption boundaries that crosscut other zones (Fig. 5d and f) and concentric zoning that truncates interior zones (Fig. 5b). For many of the grains in which the distinctive succession of dark zones in the mantle has a sharp boundary, these zones tend to truncate interior zones (Fig 5a and b). Dark, subhedral cores in some grains have irregular resorption boundaries (Fig 5a and f). A number of grains show evidence of undergoing multiple resorption events (Fig 5 d and f). Resorption features are not always observable in both grains within a pair. It is likely that they are more frequent, but the faint zoning of most grains reduces the possibility of detection.

Several zoning features are distinguished within the quartz grains. In our descriptions, based on morphologically distinct domains within grains, we use the terms core for the innermost domain, rim for the outermost domain, and mantle for the intermediary domain between the core and rim (consistent with terms used in Wiebe et al. 2007).

- Most quartz grains have indistinct, medium intensity zoning in the interior. Thin, faint oscillatory zoning is observable within some grain interiors.
- A dark core in one or both of the grains within a grain pair (~20 grains). Approximately 12 of these cores are anhedral, suggesting they underwent resorption events. Grains with dark cores may be attached to other grains with dark cores (two pairs), but are usually attached to grains without visible dark cores, although the apparent absence of cores in these grains may be the result of two-dimensional slicing.

- A thin zone that is brighter than all others is present in ~20 grains. This bright zone occurs nearer the rim of some grains and nearer to the core in others. It does not necessarily occur in both grains within a pair.
- A succession of relatively dark zones in the mantle of the grain, which range in width from 50-250 μm. This pattern occurs in both grains of ~50 pairs and in only one grain of ~35 pairs.
- Pairs of quartz grains sharing common zoning patterns in their outermost mantles (~34 pairs), an indication that the grains continued to crystallize after attachment. This paired growth is sometimes associated with resorption boundaries.

EBSD Analysis

Results from the EBSD analyses of 187 grain pairs are presented in Appendix 1 (Supplementary Materials) and Figure 6. The angles between c-axes for most grains in a pair were ~0º or ~76º. All but one of the grain pairs with c-axes oriented ~0º to each other have parallel dipyramidal faces and are thus interpreted to be in parallel orientation (Fig. 6; Fig. 7). Fifty of sixty pairs with c-axes oriented ~76º apart have one set of attached dipyramidal faces and another set oriented ~27º apart, corresponding to the Esterel twin law for quartz (Fig. 6; Fig. 7). Of those grain pairs in either Esterel twin or parallel orientation, CL imaging reveals disparate growth histories for all but three pairs (for which zoning was too faint to interpret). This indicates that the grains joined together with matched dipyramidal faces after individual crystallization. Furthermore, 21% of the grains were found to have c-axes orientations of ~84° apart, a c-axes orientation analogous to quartz twinned according to the Japanese twin law (Kozu and Machiba, 1937). However, no parallel faces were found for pairs in this orientation.

Grains would have initially come into contact as β-quartz and then transitioned into low α-quartz as the crystals cooled. Thus, adjoining crystal lattice orientations would have been distorted during this transition and then likely further distorted during compaction or post-emplacement deformation. Because of these misorientations in the lattice structures of attached crystals, those pairs with their c-axes and dipyramidal faces oriented 0-11º apart were interpreted to be in parallel orientation. Esterel twin orientations were assigned to those pairs with c-axes oriented 69-83º apart, with poles to half of the dipyramidal faces ~parallel, and with the other half oriented ~27º apart.

The majority of grain pairs, 61%, were found to be in Esterel twin or parallel orientation (Table 1). Parallel pairs were more common than Esterel twin pairs. The most common cluster size was two grains, although some clusters contained up to eight grains. Clusters with at least one grain pair in either parallel or Esterel twin orientation are much more common (78% of clusters) than those clusters without any grain pairs in either of these orientation.

DISCUSSION

Origin of the Kaharoa plutonic lithics

Our study of quartz clusters in the Kaharoa plutonic lithics builds upon a tradition of using monomineralic clusters to interpret crystallization dynamics. For example, Drugman (1927) observed that parallel and twin orientations were common in clusters of quartz from porphyry and common relative crystal orientations have also been examined in aggregates of Kilauea Iki olivine crystals (Schwindinger and Anderson, 1989). In addition, experimental studies indicate that parallel and twin oriented grain pairs can form due to dynamic processes. For instance, Gaubert (1896) found that when he shook octahedral crystals of lead nitrate in

solution, the crystals tended to cluster and to attach together in either parallel orientation or in accordance with the spinel twin law. Later, Schaskolsky and Schubnikov (1933) settled octahedral crystals of alum through a supersaturated alum solution onto a large alum face. When they stirred the solution, they found that most of the crystals were removed from the alum face. The remaining crystals attached to the plate were either attached in an orientation that corresponded to parallel growth or to the Spinel twin. Thus, the combined applied and experimental research suggest that dynamic processes within a magma system may result in like-crystals coming together in parallel and twin orientations, a phenomena termed synneusis (Vogt, 1921; Vance, 1969).

Limited studies of crystal aggregation in igneous systems indicate that monomineralic clusters form due to dynamic processes in a magma system. Beane and Wiebe (2012) studied quartz clusters from Vinalhaven, Maine in a granite and porphyry, which is interpreted to have formed from partial rejuvenation of a portion of the granite body (Wiebe et al., 2004). Previous research using CL imaging of the quartz clusters showed that the clusters were formed of quartz crystals with dissimilar growth histories, indicating that the quartz clusters in both the granite and porphyry formed after the crystallization of individual quartz grains (Weibe et al., 2007). Furthermore, they found that the zoning in the porphyry quartz recorded a large partial remelting event, while the zoning of the granite quartz did not record such an event (Wiebe et al., 2007). Using EBSD analysis, Beane and Wiebe (2012) found that all the grain pairs in the porphyry quartz clusters were in either parallel or Esterel twin orientation, though only a small percentage of the grain pairs in the coarse granite (~10%) were in either of these two orientations.

Comparing the EBSD orientation results with the CL zoning patterns in the granite and porphyry quartz, they concluded that crystals with separate growth histories had come together after crystallization and became aligned in these preferred orientations due to compaction and/or hindered settling. Because the preferred orientations of grains within quartz clusters was significantly more common in the porphyry than the granite, Beane and Wiebe (2012) concluded that these orientations were not necessarily common for quartz grain pairs in isolated magmatic systems. However, those quartz grains that are oriented with their lattice structures aligned (i.e. such as in parallel or Esterel twin orientation) likely would become strongly bonded, consistent with lead nitrate crystal stirring experiments of Gaubert (1896). Thus, when dynamic processes occur that lead to magma rejuvenation, quartz pairs in either of these orientations are less likely to be fully dissolved and separated. Thus, a high percentage of grain pairs in quartz clusters that are oriented in parallel or Esterel twin orientation indicates that crystal accumulation occurred in a dynamic environment such as a crystal mush where there is the movement of magma to allow for partial dissolution of quartz crystals and preferential preservation of oriented clusters.

Accordingly, the dominance of quartz clusters with grain pairs in either parallel or Esterel twin orientation in the Kaharoa plutonic lithics indicates that at least one dynamic process (i.e., compaction, hindered setting, or shear) occurred at shallow crustal levels, causing the quartz grains to rotate and attach in these particular orientations. Furthermore, the CL images record the effects of multiple resorption events during the formation of the Kaharoa plutonic lithics. Resorption features, detected in ~32 grains, do not all occur near the same CL intensity zones, and sometimes affect multiple zones within one grain, suggesting that multiple resorption events occurred before the solidification. These resorption features are likely the result of magma

recharge and remobilization, which also led to the preferential preservation of quartz grain pairs in parallel or Esterel twin orientation.

The results from EBSD and CL analyses indicate that the Kaharoa plutonic lithics formed as part of a shallow crystal mush which was periodically rejuvenated and partially remelted, resulting in continued crystal-liquid separation (leading to the development of a silicic cumulate). The CL evidence for multiple resorption events rules out the possibility that the Kaharoa plutonic lithics could have formed as part of an incremental magma injection that remained isolated from subsequent injections in the shallow crust. Thus, this Kaharoa case does not fit existing models for slow incremental pluton growth (with subsolidus cooling in between recharge) and temporally unrelated rhyolite formation (e.g., Glazner et al., 2004; Glazner et al., 2008; Tappa et al., 2011). The differences in growth histories within quartz grain pairs eliminates the possibility that the Kaharoa plutonic lithics represent sidewall crystallization in the magma chamber. Instead, the spatial distribution of grains within the rock is consistent with textural disequilibrium, where grains are clustered rather than ordered, indicative of the processes of crystal gathering and/or accumulation (Wager et al., 1960; Wickham, 1987; Miller et al., 1988).

Formation of high-silica rhyolite in the OVC

Our interpretation that the Kaharoa lithics represent a shallow crystal cumulate mush is supported by previous work in the TVZ, which has shown that assimilation-fractional crystallization (AFC) operates at shallow crustal levels (e.g. Wilson et al., 2006; Deering et al., 2011a). Mechanistically, a number of workers have invoked the ‘mush’ model, in which an intermediate composition crystal mush in the upper crust is capped by a crystal-poor, high

viscosity, and highly eruptible rhyolitic melt lense, extracted through processes such as hindered settling and/or compaction (e.g., Bachmann and Bergantz, 2004; Hildreth, 2004).

Evidence supporting this model comes from infrequent but large (50-5000 km^3) eruptions of unzoned, crystal-rich ignimbrites (Bachmann and Bergantz, 2004), representing erupted crystal mush zones. Such intermediate mush zones are fed by magma inputs from deeper in the crust, and rhyolite melt is extracted and stored in cupolas in the shallow crust until they freeze or erupt (Hildreth, 2004; Walker et al., 2007). An optimal melt extraction window of 50-70% crystallinity was predicted for such a system (Dufek and Bachmann, 2010). The 'mush' model reconciles a number of issues including: (1) sudden compositional gaps in ignimbrites, (2) the presence of juvenile clasts with cumulate signature capping dominantly crystal-poor rhyolitic ignimbrite (Bacon and Druitt, 1988; Deering et al., 2011c; Pamukcu et al., 2013; Bachmann et al., 2014), (3) large low velocity zones below active calderas (Dawson et al., 1990; Husen et al., 2004; Zollo et al., 2008), (4) the large observed age ranges of zircons in silicic magmas (Bachmann and Bergantz, 2004; Walker et al., 2007; Simon et al., 2008; Wotzlaw et al., 2013), and (5) trace element evidence of crystal accumulation and melt segregation in zones of plutonic complexes (Gelman et al., 2014, Lee and Morton, 2015).

In the central TVZ, gaps in composition of eruptible products have been explained through the application of this 'mush' model, an interpretation supported by radiogenic isotopes, whole-rock and mineral geochemistry, and numerical simulations of magma reservoirs (Deering et al., 2008 and 2011a). Yet, this model does not predict any significant additional crystal-liquid separation, or formation of a crystal laden mush, after the initial production of high-silica rhyolite from an intermediate magma. While a number of studies in the TVZ have suggested

some amount of crystal fractionation in the rhyolitic magmas (e.g. Brown et al., 1998; Schmitz and Smith, 2004; Wilson et al., 2006; Deering et al., 2011b), it remains unclear how important a role crystal fractionation, and particularly crystal accumulation, plays in the generation of high-silica rhyolite following its extraction from an intermediate mush in the mid- to upper-crust.

If our interpretation that the Kaharoa plutonic lithics originated via crystal fractionation in a shallow, low-silica rhyolite mush is correct, then this suggests that the 'mush' model as applied to the OVC must include an additional step of crystal fractionation as a melt-rich, high-silica rhyolite is extracted from a low-silica rhyolite mush (Fig. 9). To determine whether the Kaharoa plutonic lithics and their host rhyolite can be formed from the same low-silica rhyolite mush at shallow depths, we applied a series of thermodynamic Rhyolite-MELTS models to a representative bulk-rock composition of Kaharoa granodiorite. The bulk-rock composition used in this study (Deering, unpublished data) is nearly identical to sample TW1 from Brown et al. (1998). We used an iterative approach to matching the resultant mineral assemblages of the crystal and liquid products with those of the Kaharoa plutonic lithics and the OVC rhyolites (Fig. 8) by changing the P and H_2O conditions within the range previously determined by work in the OVC (Smith et al., 2005; Johnson et al., 2011; Begue et al., 2014; Pressure: 100 to 200 MPa, log fO_2: ~1.0 ΔQFM, and H_2O: 4-6 wt.%.). The changes in P and/or H_2O within this range lead to differences of ±10 % crystallinity of the magmatic system at the point where high-silica rhyolite is in equilibrium with the crystals. However, the following conditions were found to best match the near-solidus modal mineralogy observed in the Kaharoa granodiorite plutonic lithics and the temperature range of high-silica rhyolite erupted from the OVC: P: 150 MPa, fO_2: 1.0 ΔQFM, H_2O: 5wt.%,. The result of this model is presented in Figure 8. A detailed comparison between the

modeled rhyolite composition and the natural samples from the OVC cannot be made due to the Rhyolite-MELTS models' inability to capture the true composition of the feldspars, which influences the resultant melt composition, and the wide range of CaO, K_2O, Na_2O, and Al_2O_3 observed in the OVC rhyolite over the timespan that the granodiorite magma was hypersolidus.

The results of this thermodynamic modeling and the phase assemblage compositional information from the QEMSCAN images were used to guide interpretation and develop the subsequent model of the processes that occurred in the shallow magma system. In the Kaharoa plutonic lithics, alkali feldspar is exclusively interstitial, while this mineral is not present in any of the OVC rhyolites (Smith et al., 2005; Deering et al., 2011a, b). Consequently, if the Kaharoa plutonic lithics are part of a crystal cumulate mush from which a melt like the Kaharoa rhyolites could have formed, melt extraction from the mush must have ceased by the onset of alkali feldspar crystallization at ~55-60% crystallinity. In addition, the liquid phase composition does not reach high-silica rhyolite until ~25% crystallinity, as indicated by the onset of quartz crystallization.

Therefore, modeling guided by QEMSCAN images predicts that high-silica rhyolites may form through interstitial melt extraction from a low-silica rhyolite of ~25-60% crystallinity in the shallow crust. This range in crystallinity is slightly lower than the 50-70 crystal vol% window predicted by Dufek and Bachmann (2010) for interstitial melt extraction from basalts, andesites, and dacites. However, the higher viscosities ($10^{3.7}$ to $10^{5.4}$ Pa s; Scaillet et al., 1998) of a rhyolitic melt and the cold conditions in the upper crust would inhibit melt extraction at higher crystallinity, slowing down hindered settling and/or compaction processes.

The much lower limit predicted by Rhyolite-MELTS for the extraction window may be too low as it is not specifically calibrated for TVZ compositions and, at 25% crystallinity, there

would be very little quartz crystallization. Because the Kaharoa plutonic lithics consist of large quartz phenocrysts (1 to 5 mm), we suggest that the lower limit of melt extraction is likely closer to 35-40% crystallinity. Regardless of the precise lower limit when crystal liquid separation began, the CL and EBSD evidence for cumulate formation at shallow depths and the good fit for crystal fractionation models to produce high-silica rhyolite melt between >25-30 to 60 vol.% crystals from a low-silica rhyolite melt imply that when the 'mush' model of rhyolite formation is invoked for the OVC, and possibly elsewhere, it should include an additional step in which high-silica, crystal-poor rhyolite is extracted from a low-silica rhyolite mush at very shallow crustal levels (~100-150 MPa; Fig. 9) in the most active magmatic provinces.

Longevity of cumulates in the OVC

Late-stage crystallization of the Kaharoa plutonic lithics is recorded by the growth zones in the outer portions of the quartz grains. CL imaging shows that all quartz grains are typically normally zoned (as are the plagioclase). Also many quartz grains exhibit shared late-stage crystal growth, indicated by the characteristic succession of dark CL zones in the mantle of ~135 grains and the occurrence of zoning patterns which encompass entire grain pairs. These patterns indicate that much of the later stage crystallization in this portion of the mush was uninterrupted by recharge events. This may be because the final stage of solidification occurred during a time: 1) of quiescence, or very high crystallinity, in the magma system, 2) when this portion of the cumulate became thermally isolated from regions of magma recharge, or 3) punctuated by rapid solidification occurring in the underlying magmatic system induced by eruption (Bachmann et al., 2012).

Studies of zircon U-Th dating of the Kaharoa plutonic lithics indicate that the timing of solidification of the lithics was not one of quiescence at the OVC even though it occurred prior to the Kaharoa eruptive episode at 0.7 ka. Zircon crystallization in the Kaharoa plutonic lithics ranges from ~300 to 125 ka (Shane et al., 2012) and this period was one of frequent and intense volcanism at the OVC (Cole et al., 2014). Therefore, rather than reflecting a time of quiescence in the magma system, the crystallization of quartz phenocrysts within the Kaharoa plutonic lithics reflect that thermal isolation occurs in regions of a magmatically active system, indicative of synchronicity between plutonism and volcanism at the OVC. Such results are consistent with inferences from other studies which indicate: (1) synchronous growth of plutons in the TVZ (Brown et al., 1998; Burt et al., 1998; Charlier et al., 2005; Cole et al., 2014), (2) the scavenging of antecrysts (Klemetti et al., 2011), and (3) the storage of a shallow crystal mush at temperatures near or at the solidus for a majority of its 'lifetime' (possibly >90% of the time; Cooper and Kent, 2014).

IMPLICATIONS

The study of quartz clusters in plutonic lithics provides new insights into the plutonic processes occurring in active volcanic complexes such as the OVC. When discussed in the context of previous studies and proposed models, the results from combined QEMSCAN imaging, CL imaging and electron backscatter diffraction show that the Kaharoa plutonic lithics formed by crystal accumulation in a mush at very shallow crustal levels, rather than in-situ along the carapace or during an isolated magma injection (Deering et al., 2012; Shane et al., 2012). These results have implications for models of rhyolite generation in the OVC, TVZ, and elsewhere. While other studies of the TVZ rhyolites are consistent with extraction from an

intermediate magma as proposed by Bachmann and Bergantz (2004) and Hildreth (2004), the evidence here suggests a final stage of differentiation is occurring to produce the highest silica, crystal-poor rhyolites found in magmatic systems. Although the predicted window for melt extraction in this final stage is of lower crystallinity (>25-60%) than previously predicted by numerical modeling melt-crystal dynamics (~50-70%; Dufek and Bachmann, 2010), extraction at a lower crystallinity may occur due to the higher viscosities involved in this terminal stage. Finally, the Kaharoa plutonic lithics represent direct evidence that portions of a large crystal mush may be near or sub-solidus for prolonged periods of time despite continuing volcanic activity. Hence, the shallow magma system of the OVC can be envisioned as a long-lived crystal mush in a near solidus state from which high-silica rhyolite melt is periodically extracted due to reheating and remobilization from a low-silica rhyolite melt and stored in roof lenses until eruption.

ACKNOWLEDGEMENTS

Funding was provided in part by NSF awards 1249821, 9951390, and 0320871, and Bowdoin College Surdna and Grua/O'Connell awards. Special thanks to the Frontiers Abroad program for the opportunity to begin this research, and to R.A. Wiebe for his insightful ideas about synneusis in magma chambers. Generous assistance from F. Bégué, S. Gelman, K. Kunze, K. Pfaff and K. Swanson during data collection and analysis is much appreciated. K. Cooper, A. Glazner, C. Miller, E. Peterman, and R.A. Wiebe provided thoughtful reviews that greatly improved the manuscript.

FIGURE CAPTIONS

Figure 1. Map of the Okataina Volcanic Complex (OVC) located within the central Taupo Volcanic Zone of the North Island, New Zealand. The solid line outlines the main volcanic centers. The dashed

line outlines major ignimbrite and tephra deposits in Puhipuhi basin. Inset shows location of the OVC on the North Island. From Hannu Seebeck, personal communication.

Figure 2. Cathodoluminescence and EBSD analysis on Kali102A_5 cluster 3. (I) CL image reveals two distinct quartz grains with separate cores and growth histories. Light zones correspond to higher Ti reflecting higher temperature growth conditions (Wark and Watson, 2006). (II) Upper hemispheric stereographic projections of the quartz grain orientations; Red dots indicate orientation of grain **a** and green dots indicate that of **b**. The left plot shows the c-axes orientations of each grain while the other two plots show orientations of the grain's dipyramidal faces. The c-axes for these grains are oriented 77° apart, one set of dipyramidal faces are nearly parallel, and the other is oriented ~27° apart consistent with Esterel twin orientation. (III) Visual representation of the orientation of grains **a** and **b**. Note that the grains have dipyramidal faces, which are not shown.

Figure 3. QEMSCAN images of thin sections KaLi102A_2 and KaLi4A_4. **(A)** Phase assemblage maps. Quartz (pink) and plagioclase feldspar (pale blues) occur primarily as phenocrysts while alkali feldspar (dark blue) is only interstitial. Plagioclase with $An_{40\text{-}100\%}$ is represented as anorthite while plagioclase with $An_{0\text{-}40\%}$ is represented as albite. Mafic minerals are almost entirely biotite. **(B)** Total mineral contents of each sample by percent volume: 37-38% quartz, 28-29% albite, 6-7% anorthite, 20-22% alkali feldspar, 2.5-3% muscovite, 2-3.2% biotite, and 0.3-0.4% other minerals. Modal mineralogy varies no more than 2% per mineral between the two samples.

Figure 4. QEMSCAN plagioclase compositional maps showing only the feldspar phases of KaLi102A_2 and KaLi4A_4. These images highlight the interstitial nature of the alkali feldspar and the albitic overgrowths on the plagioclase phenocrysts. Compositional bins: Albite (An_0); An_{20} ($An_{1\text{-}20}$); An_{40} ($An_{20\text{-}40}$); An_{60} ($An_{40\text{-}60}$); An_{80} ($An_{60\text{-}80}$); Anorthite ($An_{80\text{-}100}$).

Figure 5. CL images with traced copies that highlight CL intensity zoning. (A) Image of KaLi102A_2 cluster 5 shows resorbed dark core in center grain. All grains show darkly zoned rims. (B) Kali102A_2 cluster 5. Upper left grain exhibits partial resorption along right grain boundary. Lower left grain shows inner zones truncated by the darker outer zones. (C) KaLi4A_2 cluster 11 consists of three grains. Two of the grains have dark, partially resorbed cores, one in the top left and the other in the top right, that are now in contact. An additional grain in lower right has a bright truncated zone at the grain boundary. Because the cores of these grains are touching, these resorption events must have occurred prior to the grains attaching. (D) Kali4A_4 cluster 5 consists of 4 grains. The upper three grains appear to have attached before the event resulting in the bright white zone because this zone did not form between each grain. The lower grain appears to have attached after the growth of the darker outer zone, because the bright zone and dark zone formed between this grain and the one above it. In all grains, the dark zone truncates interior zones, indicating a resorption event. (E) KaLi102A_2 cluster 4 consists of three grains, a large grain on the left and two small grains on the right. The zoning in the two small grains is truncated near the boundary of the larger grain. This suggests that these grains were partially resorbed before attaching to the larger grain. (F) KaLi102A_5 cluster 5 shows three distinct grains. The lower right grain records two resorption events: one that resorbed the core and another associated with the outer zone.

Figure 6. Histogram showing the frequency of the relative angles measured between the c-axes of quartz grain pairs. Grain pairs are defined as those grains that are touching or separated by less than 250μm of interstitial alkali feldspar. Left and right blue boxes enclose those grains determined to be in parallel and Esterel twin respectively.

Figure 7. Schematic of preferred quartz grain orientations. Redrawn from Figure 1 of Beane and Wiebe (2012).

Figure 8. Graph showing Rhyolite-MELTS modeled evolution for a shallow, low-silica rhyolite (granodiorite) melt system. Modeling conditions: Pressure: 150 MPa, log fO_2:1.0 ΔQFM, and H_2O: 5 wt.%, represent those determined to be the 'best-fit'; see text for discussion. Mass of the system is approximately 100g and thus can be used as a proxy for percent crystallinity. The pink box shows the window of melt crystallinity, found from the model, for which high-silica rhyolite may be extracted. This is bound by the crystallinity at which quartz begins to crystallize (~25%), and the crystallinity at which alkali feldspar begins to crystallize (~60%).

Figure 9. Schematic of modified 'mush' model. Inset shows accumulation of quartz crystals in the remobilized low-silica mush. As crystals undergo hindered settling, dipyramidal quartz grains rotate and attach along parallel dipyramidal faces, and interstitial, high-silica rhyolite melt is extracted.

Table 1. Summary of orientation results.

Supplementary material: EBSD results. Relative angle in degrees between c-axes and dipyramidal faces of quartz grain pairs in clusters from the Kaharoa plutonic lithics. Chemical variations, which are used to interpret growth histories, of each grain were imaged using CL. Grain pairs that were analyzed but whose grains were too far apart are excluded from the results and this table. "Separate grains?" column indicates those quartz grain pairs in which the grains have separate growth histories.

REFERENCES

Bachmann, O. (2010) The petrologic evolution and pre-eruptive conditions of the rhyolitic Kos Plateau Tuff (Aegean Arc). Central European Journal of Geosciences, 2(3), 270-305.

Bachmann, O., and Bergantz, G.W. (2004) On the origin of crystal-poor rhyolites: Extracted from batholithic crystal mushes. Journal of Petrology, 45, 1565-1582.

Bachmann, O., Deering, C.D., Ruprecht, J.S., Huber, C., Skopelitis, A., and Schnyder, C. (2012) Evolution of silicic magmas in the Kos-Nisyros volcanic center, Greece: cycles associated with caldera collapse. Contributions to Mineralogy and Petrology, 163(1), 155-166.

Bachmann, O., Deering, C.D., Lipman, P.W., and Plummer, C. (2014) Building zoned ignimbrites by recycling silicic cumulates: insight from the 1,000 km^3 Carpenter Ridge Tuff, CO. Contributions to Mineralogy and Petrology, 167, 1025.

Bacon. C.R., and Druitt, T.H. (1988) Compositional evolution of the zoned calcalkaline magma chamber of Mount Mazama, Crater Lake, Oregon. Contributions to Mineralogy and Petrology, 98, 224-256.

Bacon, C.R., and Lowenstern, J.B. (2005) Late Pleistocene granodiorite source for recycled zircon and phenocrysts in rhyodacite lava at Crater Lake, Oregon. Earth and Planetary Science Letters, 233(3), 277-293.

Beane, R., and Wiebe, R. (2012) Origin of quartz clusters in Vinalhaven granite and porphyry, coastal Maine. Contributions to Mineralogy and Petrology, 163(6), 1069-1082.

Bégué, F., Gualda, G., Giorso, M., Paukcu, A., Kennedy, B., Gravley, D., Deering, C., and Chambefort, I. (2014) Phase-equilibrium geobarometers for silicic rocks based on rhyolite-MELTS. Part 2: application to Taupo Volcanic Zone rhyolites, Contributions to Mineralogy and Petrology, 168, 1082-1098.

Brown, S.J., Wilson, C.J., Cole, J.W., and Wooden, J.L. (1998) The Whakamaru Group ignimbrites, Taupo Volcanic Zone, New Zealand: Evidence for reverse tapping of a zoned silicic magmatic system. Journal of Volcanology and Geothermal Research, 84, 1-37.

Bryan, C.J., Sherburna, S., Bibb, H.M., and Bannister, S.C. (1999) Shallow seismicity of the central Taupo Volcanic Zone, New Zealand: Its distribution and nature. New Zealand Journal of Geology and Geophysics, 42(4), 533-542.

Burt, R.M., Brown, S.J., Cole, J.W., Shelley, D., and Waight, T.E. (1998) Glass-bearing plutonic fragments from ignimbrites of the Okataina caldera complex, Taupo Volcanic Zone, New Zealand: remnants of a partially molten intrusion associated with preceding eruptions. Journal of Volcanology and Geothermal Research, 84, 209-237.

Charlier, B.L.A., Peate, D.W., Wilson, C.J., Lowenstern, J.B., Storey, M., and Brown, S.J. (2003) Crystallisation ages in coeval silicic magma bodies: 238U=230Th disequilibrium evidence from the Rotoiti and Earthquake Flat eruption deposits, Taupo Volcanic Zone, New Zealand. Earth and Planetary Science Letters, 206, 441-457.

Charlier, B.L., Wilson, C.J., Lowenstern, J.B., Blake, S., van Calsteren, P.W., and Davidson, J.P. (2005) Magma generation at a large, hyperactive silicic volcano (Taupo, New Zealand) revealed by U–Th and U–Pb systematics in zircons. Journal of Petrology, 46, 3-32.

Cole, J.W., Deering, C.D., Burt, R.M., Sewell, S., Shane, P.A., and Matthews, N.E. (2014) Okataina Volcanic Centre, Taupo Volcanic Zone, New Zealand: A review of volcanism

and synchronous pluton development in an active, dominantly silicic caldera system. Earth-Science Reviews, 128, 1-17.

Coleman, D.S., Bartley, J.M., Glazner, A.F., and Pardue, M.J. (2012) Is chemical zonation in plutonic rocks driven by changes in source magma composition or shallow-crustal differentiation? Geosphere, 8(6), 1568-1587.

Cooper, K.M., and Kent, A.J.R. (2014) Rapid remobilization of magmatic crystals kept in cold storage. Nature, 506, 480-483.

Dawson, P.B., Evans, J.R., and Iyer, H.M. (1990) Teleseismic tomography of the compressional wave velocity structure beneath the Long Valley region. Journal of Geophysical Research, 95(B7), 11021-11050.

Deering, C.D., Cole, J.W., and Vogel, T.A. (2008) A rhyolite compositional continuum governed by lower crustal source conditions in the Taupo Volcanic Zone, New Zealand. Journal of Petrology, 49 (12), 2245-2276.

Deering, C.D., and Bachmann, O. (2010) Trace element indicators of crystal accumulation in silicic igneous rocks. Earth and Planetary Science Letters, 297 (1), 324-331.

Deering C.D., Bachmann, O., Dufek, J., and Gravley, D.M. (2011a) Rift-related transition from andesite to rhyolite volcanism in the taupo volcanic zone (New Zealand) controlled by crystal-melt dynamics in mush zones with variable mineral assemblages. Journal of Petrology, 52(11), 2243-2263.

Deering, C.D., Cole, J.W., and Vogel, T.A. (2011b) Extraction of crystal-poor rhyolite from a hornblende-bearing intermediate mush: a case study of the caldera-forming Matahina eruption, Okataina volcanic complex. Contributions to Mineralogy and Petrology, 161(1),129-151.

Deering, C.D., Bachmann, O., and Vogel, T.A. (2011c) The Ammonia Tanks Tuff: erupting a melt-rich rhyolite cap and its remobilized crystal cumulate. Earth and Planetary Science Letters, 310(3-4), 518-525.

Deering, C.D., Horton, T.W., Gravley, D.M., and Cole, J.W. (2012) Hornblende, cummingtonite, and biotite hydrogen isotopes: Direct evidence of slab-derived fluid flux in silicic magmas of the Taupo Volcanic Zone, New Zealand. Journal of Volcanology and Geothermal Research, 233-234, 27-36.

Drugman, J. (1927) On β-quartz twins from some Cornish localities. Mineral Magazine, 21, 366-382.

Dufek, J., and Bachmann, O. (2010) Quantum magmatism: Magmatic compositional gaps generated by melt-crystal dynamics. Geology, 38(8), 687,690.

Fynn, G.W., and Powell, W.J.A. (1979) The cutting and polishing of electro-optic materials. Adam Hilger, London

Gelman, S.E., Deering, C.D., Bachmann, O., Huber, C. & Gutierrez, F.J. (2014) Identifying the crystal graveyards remaining after large silicic eruptions. Earth and Planetary Science Letters 403, 299-306.

Gaubert, P. (1896) Sur la production artificielle de la macle des spinelles dans les cristaux d'azotate de plomb. Bulletin for the Society of French Mineralogy, 19, 431-434.

Glazner, A.F., Bartley, J.M., Coleman, D.S, Gray, W., and Taylor, R.Z. (2004) Are plutons assembled over millions of years by amalgamation from small magma chambers? GSA Today, 14, 1052-5173.

Glazner, A.F, Coleman, D.S., and Bartley, J.M. (2008) The tenuous connection between high-silica rhyolites and granodiorite plutons. Geology, 36(2), 183-186.

Hildreth, W. (2004) Volcanological perspective on Long Valley, Mammoth Mountain, and Mono Craters: several contiguous but discrete systems. Journal of Volcanology and Geothermal Research, 136(3), 169-198.

Hildreth, W., and Wilson, C. (2007) Compositional zoning of the Bishop Tuff. Journal of Petrology, 48, 951-999.

Husen, S., Smith, R.B., and Waite, G.P. (2004) Evidence for gas and magmatic sources beneath the Yellowstone volcanic field from seismic tomographic imaging. Journal of Volcanology and Geothermal Research, 131(3-4), 397-410.

Keller, J. (1969) Origin of rhyolites by anatectic melting of granitic crustal rocks; the example of rhyolitic pumice from the island of Kos (Aegean sea). Bulletin Volcanologique, 33(3), 942-959.

Klemetti, E.W., Deering, C.D., Cooper, K.M., and Roeske, S.M. (2011) Magmatic perturbations in the Okataina Volcanic Complex, New Zealand at thousand-year timescales recorded in single zircon crystals. Earth and Planetary Science Letters, 305, 185-194.

Kozu, S., and Machiba, I. (1937) A discussion on the fundamental types of twining and structure of composition planes and its neighborhood from etching. Japanese Journal of Mineralogy Petrology and Economic Geology, 17, 53-95 (in Japanese).

Krieger-Lassen, N.C. (1995) The relative precision of crystal orientations measured from electron backscattering patterns. J Microscopy, 181, 72–81.

Lee, C.T.A., and Morton, D.M. (2015) High silica granites: Terminal porosity and crystal settling in shallow magma chambers. Earth and Planetary Science Letters 409, 23-31.

Leonard ,G.S., Cole, J.W., Nairn, I.A., and Self, S. (2002) Basalt triggering of the c. AD 1305 Kaharoa rhyolite eruption, Tarawera volcanic complex, New Zealand. Journal of Volcanology and Geothermal Research, 15(3), 461-486.

Lowenstern, J.B., Persing, H.M., Wooden, J.L., Lanphere, M., Donnelly-Nolan, J., and Grove, T.L. (2000) U-Th dating of single zircons from young granitoid xenoliths: new tools for understanding volcanic processes. Earth and planetary Science Letters 183(1), 291-302.

Prior, D.J., Boyle, A.P., Brenker, F., Cheadle, M.C., Day, A., Lopez, G., Peruzzo, L., Potts, G.J., Reddy, S., Spiess, R., Timms, N.E., Trimby, P.W., Wheeler, J., Zetterstro¨m, L. (1999) The application of electron backscatter diffraction and orientation contrast imaging in the SEM to textural problems in rocks. American Mineralogist, 84,1741–1759.

Miller C.F., Watson, E.B., and Harrison, T.M. (1988) Perspectives on the source, segregation and transport of granitoid magmas. Transactions of the Royal Society of Edinburgh: Earth Sciences, 79, 135-156.

Müller, A., Breiter, K., Seltmann, R., and Pécskay, Z. (2005) Quartz and feldspar zoning in the eastern Erzgebirge volcano-plutonic complex (Germany, Czech Republic): evidence of multiple magma mixing. Lithos, 80, 201–227.

Nairn, I.A, Self, S., Cole, J.W., and Leonard, G.S. (2001) Distribution, stratigraphy, and history of proximal deposits from the c. AD 1305 Kahroa eruptive episode at Tarawera Volcano, New Zealand. New Zealand Journal of Geology and Geophysics, 44(3), 467-484.

Nairn, I.A., Shane, P., Cole, J.W., Leonard, G.J., Self, A., and Pearson, N. (2004) Rhyolite magma processes of the AD 1315 Kaharoa eruption episode, Tarawera volcano, New Zealand. Journal of Volcanology and Geothermal Research, 131, 265-294.

Pamukcu, A.S., Carley, T.L., Gualda, G.A.R., Miller, C.F., and Ferguson, C.A. (2013) The Evolution of the Peach Spring Giant Magma Body: Evidence from Accessory Mineral Textures and Compositions, Bulk Pumice and Glass Geochemistry, and Rhyolite-MELTS Modeling. Journal of Petrology, 54(6), 1109-1148.

Sands, D.E. (1969) Introduction to crystallography. WA Benjamin, New York.

Scaillet, B. Holtz, F., and Pichavant, M. (1998) Phase equilibrium constraints on the viscosity of silicic magmas: 1. Volcanic-plutonic comparison. Journal of Geophysical Research, 103, 27257-27266.

Schaskolsky, M., and Schubnikow, A. (1933) Uber die kunstliche Herstellung gesetzmassiger Kristallverwachungen des Kalialauns. Zeitschrift Kristallographie, 85, 1-16.

Schmidt, N.H., and Olesen, N.O. (1989) Computer-aided determination of crystal lattice orientation from electron channeling patterns in the SEM. American Mineralogist, 27, 15–22.

Schmitz, M.D., and Smith, I.E. (2004) The petrology of the Rotoiti Eruption Sequence, Taupo Volcanic Zone: an example of fractionation and mixing in a rhyolitic system. Journal of Petrology, 45(10), 2045-2066.

Schwindinger, K.R., and Anderson, A.T. (1989) Synneusis of Kilauea Iki olivines. Contributions to Mineral Petrology, 103, 187-198.

Shane, P., and Sandiford, A., (2003) Paleovegetation of marine isotope stages 4 and 3 in northern New Zealand and the age of the widespread Rotoehu tephra. Quaternary Research, 59(3), 420-429.

Shane P., Storm, A., Schmitt, A.K., and Lindsay, J.M. (2012) Timing and conditions of formation of granitoid clasts erupted in recent pyroclastic deposits from Tarawera Volcano (New Zealand), Lithos, 140-141, 1-10.

Simon, J.I., Renne, P.R., Mundil, R. (2008) Implications of pre-eruptive magmatic histories of zircons for U-Pb geochronology of silicic extrusions. Earth and Planetary Science Letters, 266(1-2), 182-194.

Smith, V.C., Shane, P.S., and Nairn, I.A. (2005) Trends in rhyolite geochemistry, mineralogy, and magma storage during the last 50 kyr at Okataina and Taupo volcanic centres, Taupo Volcanic Zone, New Zealand. Journal of Volcanology and Geothermal Research, 148, 372-406.

Storm, S., Shane, P., and Schmitt, A.K. (2012) Decoupled crystallization and eruption histories of the rhyolite magmatic system at Tarawera volcano revealed by zircon ages and growth rates. Contributions to Mineralogy and Petrology, 163(3), 505-519.

Tappa, M.J., Coleman, D.S, Mills, R., and Samperton, K. (2011) The plutonic record of a silicic ignimbrite from the Latir volcanic field, New Mexico."Geochemistry, Geophysics, Geosystems, 12(10).

Vance J.A. (1969) On synneusis. Contributions to Mineral Petrology, 24, 7-9.

Vazquez, J.A., Shamberger, P.J., and Hammer, J.E. (2007) Plutonic xenoliths reveal timing of magma evolution at Hualalai and Mauna Kea, Hawaii. Geology, 35(8), 695-698.

Vogt, J.H.L. (1921) The physical chemistry of the crystallization and magmatic differentiation of igneous rocks. Journal of Geology, 29, 318-350.

Wager, L.R., Brown, G.M., and Wadsworth, W.J. (1960) Types of igneous cumulates. Journal of Petrology, 1, 73-85.

Walker, B.J., Miller, C.F., Lowery, L.E., Wooden, J.L., Miller, J.S. (2007) Geology and geochronology of the Spirit Mountain batholith, southern Nevada: implications for timescales and physical processes of batholith construction. Journal of Volcanology and Geothermal Research, 167, 239-262.

Wark, D.A., and Spear, F.S. (2005) Ti in quartz; Cathodoluminescence and thermometry. Geochimica et Cosmochimica Acta Supplement, 69, 592.

Wark, D.A., and Watson, E.B. (2006) The TitaniQ: a titanium-in-quartz geothermometer. Contributions to Mineralogy and Petrology, 152, 743–754.

Wickham, S.M. (1987) The segregation and emplacement of granitic magmas. Journal of the Geological Society, London, 144, 281-297.

Wiebe, R.A., Manon, M.R., Hawkins, D.P., and McDonough, W.F. (2004) Late-Stage Mafic Injection and Thermal Rejuvenation of the Vinalhaven Granite, Coastal Maine. Journal of Petrology, 45(11), 2133-2153.

Wiebe, R.A., Wark, D.A., and Hawkins, D.P. (2007) Insights from quartz cathodoluminescence zoning into crystallization of the Vinalhaven granite, coastal Maine. Contributions to Mineralogy and Petrology, 154, 439-453.

Wilson C.J., Houghton, B.F., and McWilliams, M.O. (1995) Volcanic and Structural evolution of the Taupo Volcanic Zone, New Zealand: a review. Journal of Volcanology and Geothermal Research, 68(1), 1-28.

Wilson, C.J., Blake, S., Charlier, B.L., and Sutton, A.N. (2006) The 26.5 ka Oruanui Eruption, Taupo Volcano, New Zealand: Development, Characteristics and evacuation of a large rhyolitic magma body. Journal of Petrology, 47(1), 35-69.

Wilson C.J., Gravley, D.M., Leonard, G.S., and Rowland, J.V. (2009) Volcanism in the central Taupo Volcanic Zone, New Zealand: tempo, styles, and controls. Studies in Volcanology: The Legacy of George Walker. Special publications of IAVCEI, 225-247.

Wotzlaw, J.F., Schaltegger, U., Frick, D.A., Dungan, M.A., Gerdes, A., and Gunther, D. (2013) Tracking the evolution of large-volume silicic magma reservoirs from assembly to supereruption. Geology, 41, 867-870.

Zollo, A., Maercklin, N., Vassallo, M., Dello Iacono, D., Virieux, J., and Gasparini, P. (2008) Seismic reflections reveal a massive melt layer feeding Campi Flegrei caldera. Geophysical Research Letters, 35(12), L12306.

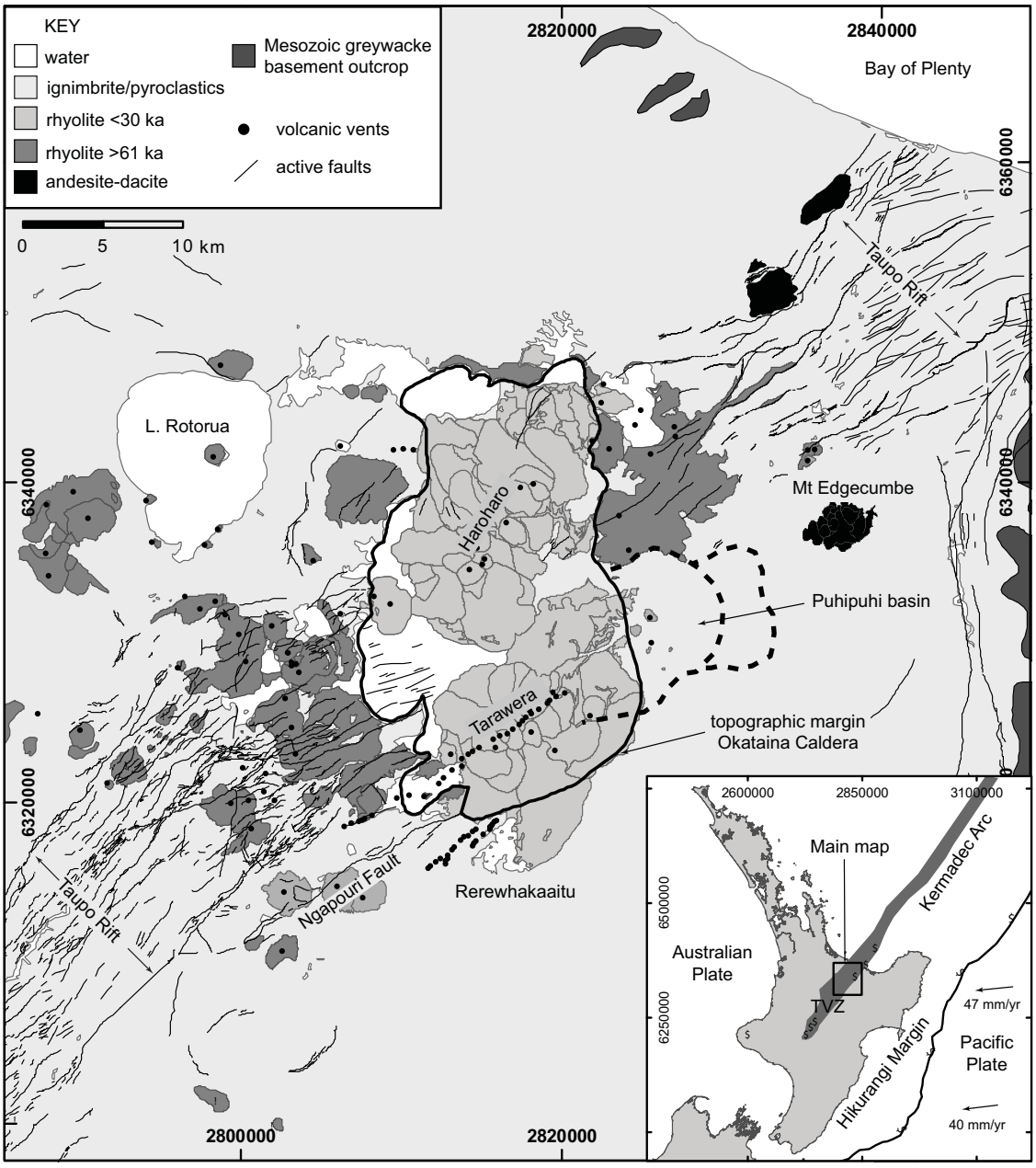
KEY
water
ignimbrite/pyroclastics
rhyolite <30 ka
rhyolite >61 ka
andesite-dacite
Mesozoic greywacke basement outcrop
volcanic vents
active faults
0 5 10 km
2820000
2840000
Bay of Plenty
6360000
Taupo Rift
L. Rotorua
6340000
Haroharo
Mt Edgecumbe
Puhipuhi basin
Tarawera
topographic margin
Okataina Caldera
6320000
Taupo Rift
Ngapouri Fault
Rerewhakaaitu
2800000
2820000
2600000
2850000
3100000
Main map
Kermadec Arc
6500000
Australian Plate
TVZ
47 mm/yr
6250000
Pacific Plate
Hikurangi Margin
40 mm/yr

Figure 1

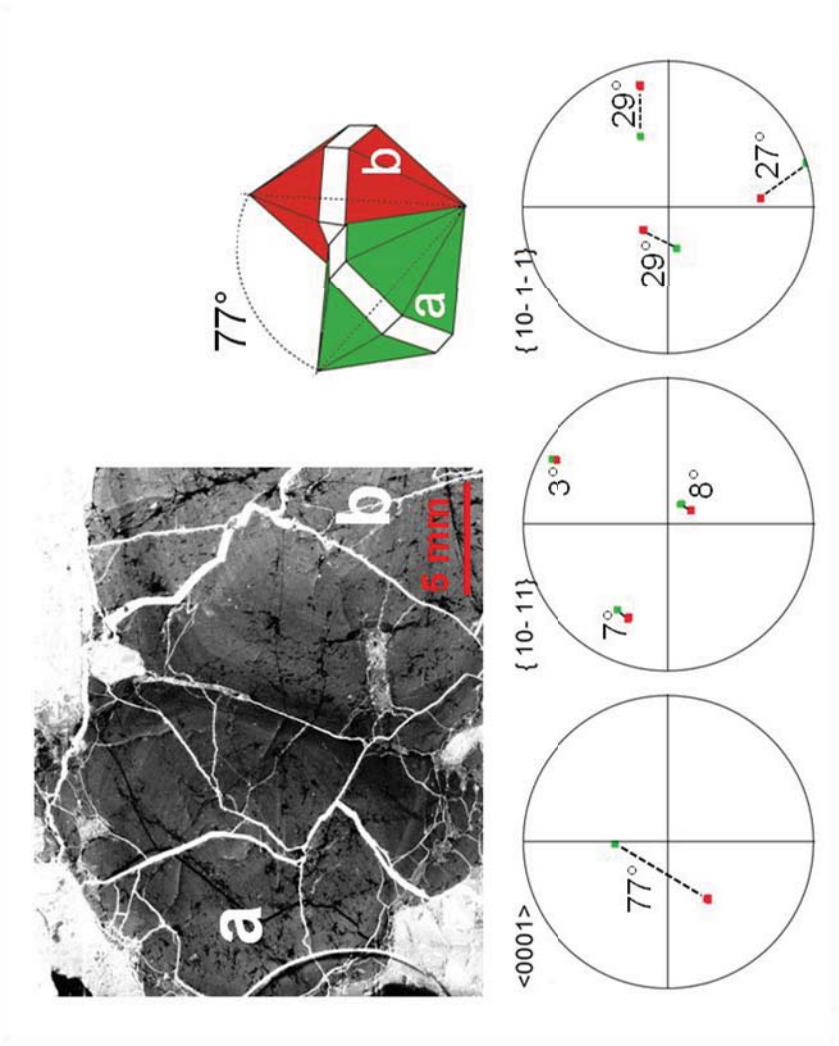
77°
b
a
5 mm
b
a
{ 10- 1- 1}
29°
29°
27°
{ 10- 11}
3°
8°
7°
<0001>
77°

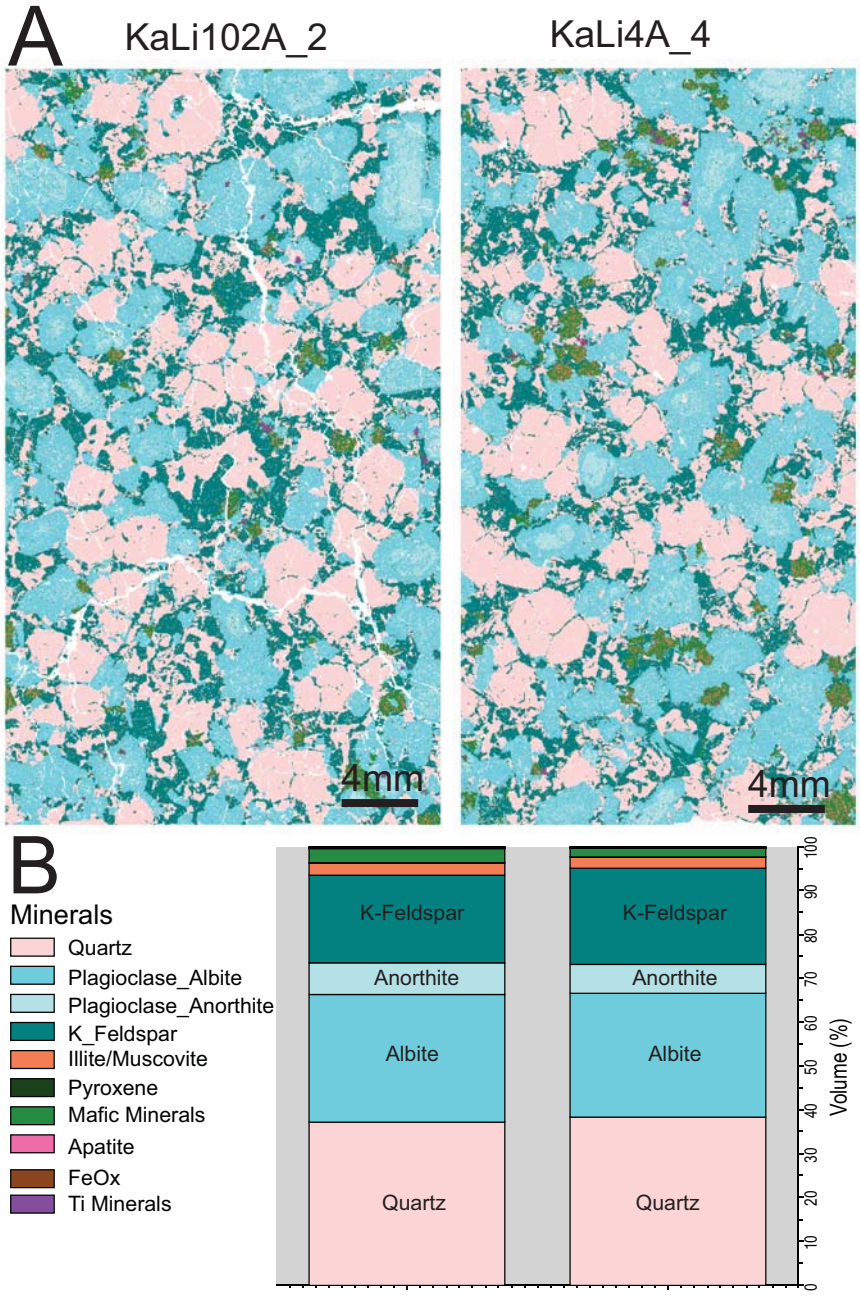
A
KaLi102A_2
KaLi4A_4
4mm
4mm
B
Minerals
Quartz
Plagioclase_Albite
Plagioclase_Anorthite
K_Feldspar
Illite/Muscovite
Pyroxene
Mafic Minerals
Apatite
FeOx
Ti Minerals
K-Feldspar
Anorthite
Albite
Quartz
K-Feldspar
Anorthite
Albite
Quartz
Volume (%)
0
10
20
30
40
50
60
70
80
90
100

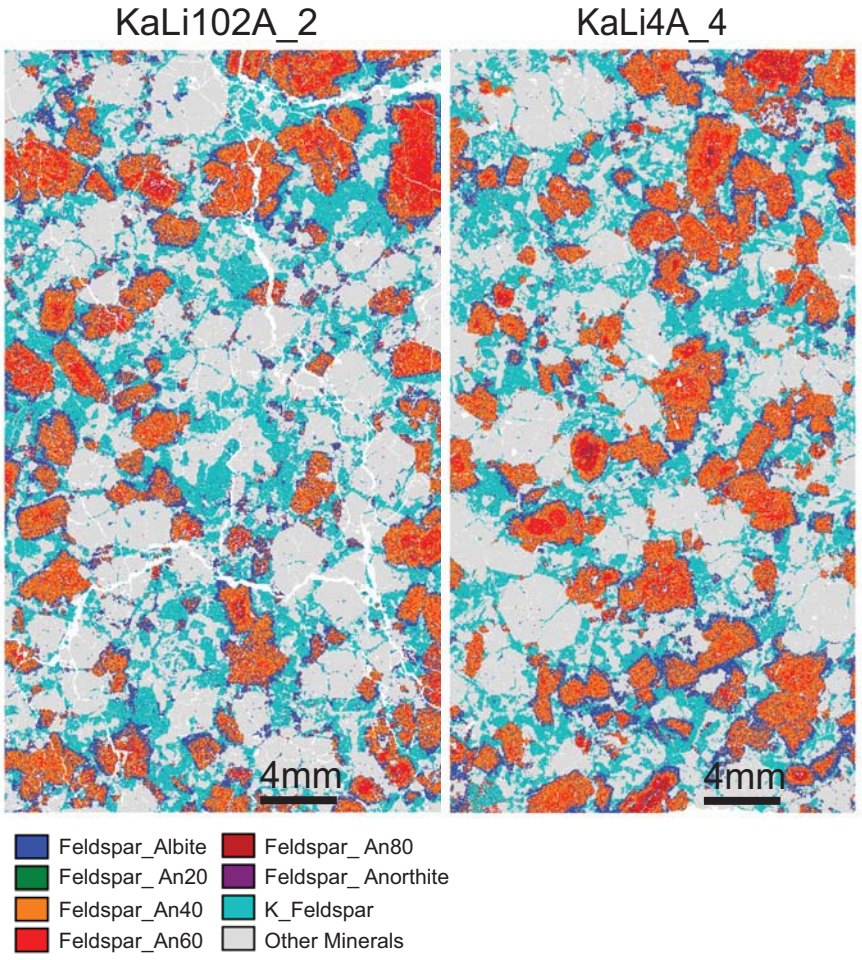
KaLi102A_2
KaLi4A_4
4mm
4mm
Feldspar_Albite
Feldspar_ An20
Feldspar_An40
Feldspar_An60
Feldspar_ An80
Feldspar_ Anorthite
K_Feldspar
Other Minerals

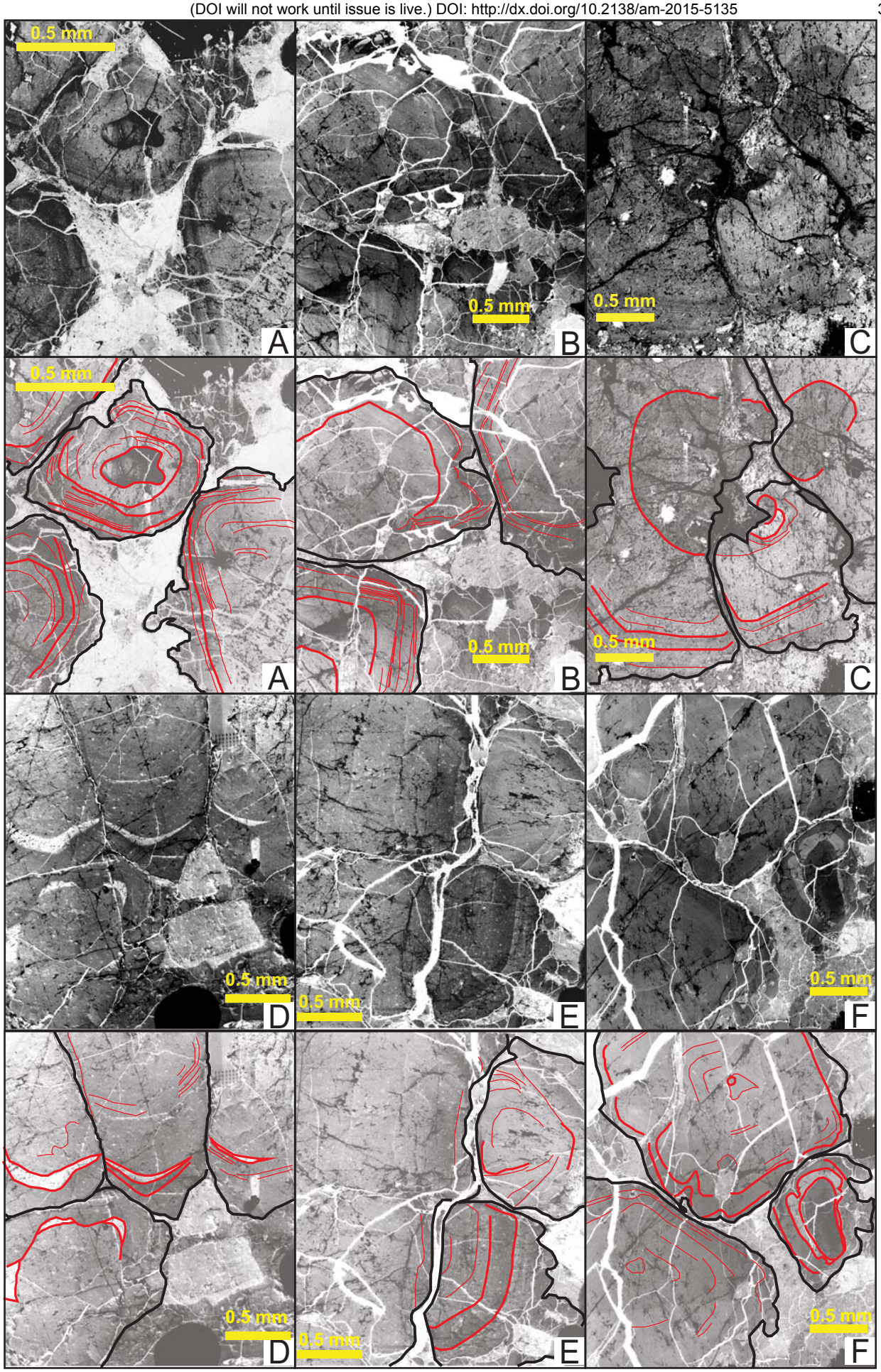
0.5 mm
A
0.5 mm
B
0.5 mm
C
0.5 mm
A
0.5 mm
B
0.5 mm
C
0.5 mm
D
0.5 mm
E
0.5 mm
F
0.5 mm
D
0.5 mm
E
0.5 mm
F

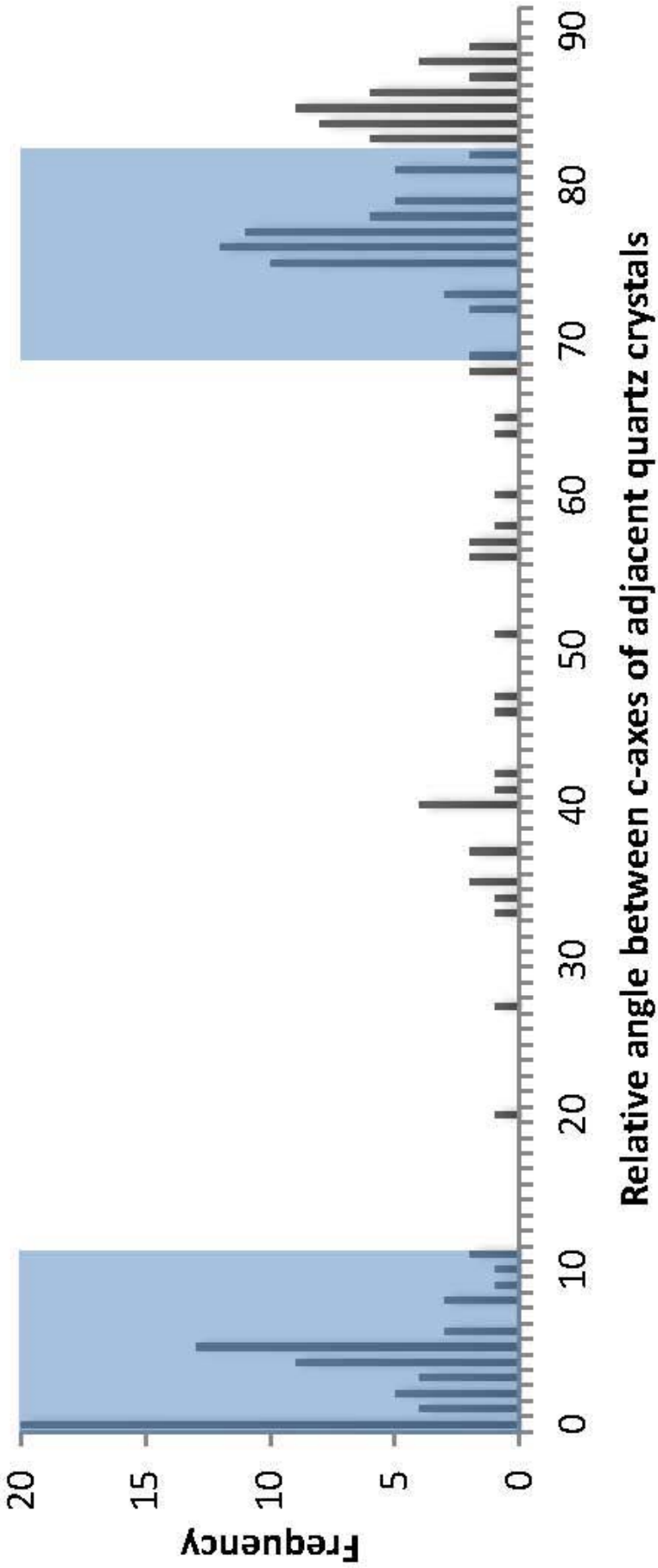
Frequency
0
5
10
15
20
0
10
20
30
40
50
60
70
80
90
Relative angle between c-axes of adjacent quartz crystals

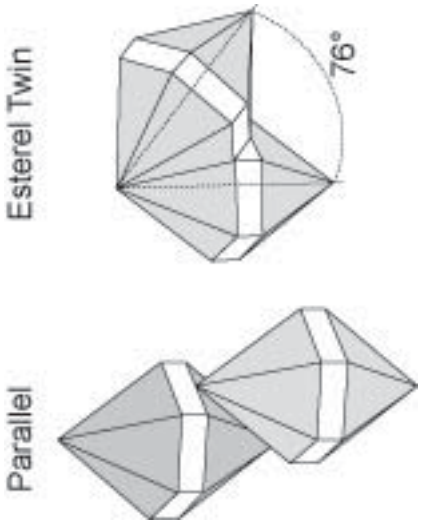
Esterel Twin
76°
Parallel

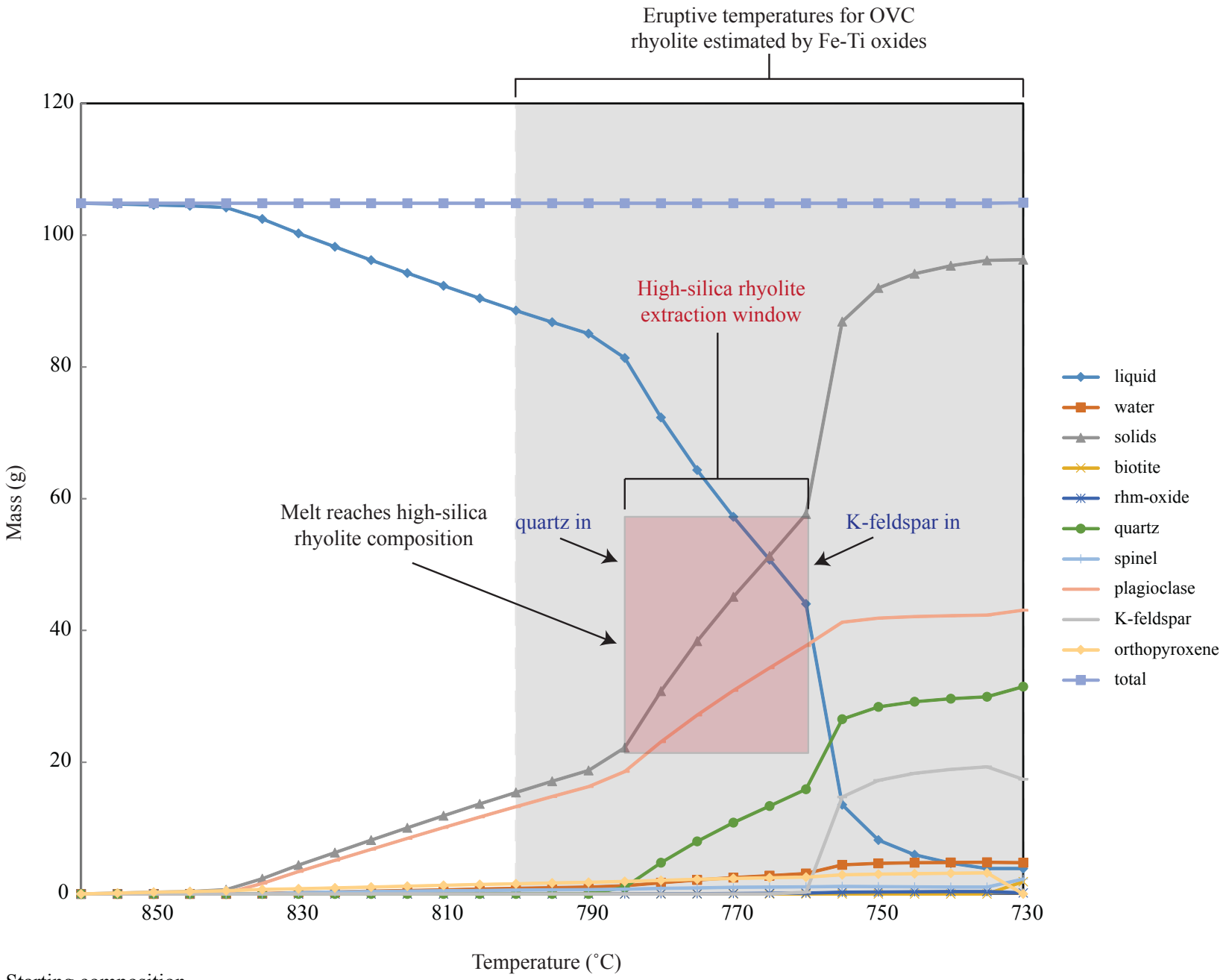

Starting composition

	SiO_2	TiO_2	Al_2O_3	Fe_2O_3	MnO	MgO	CaO	Na_2O	K_2O	P_2O_5	Total
UC970	73.41	0.26	14.14	2.27	0.08	0.55	2.02	4.29	2.94	0.05	100.00

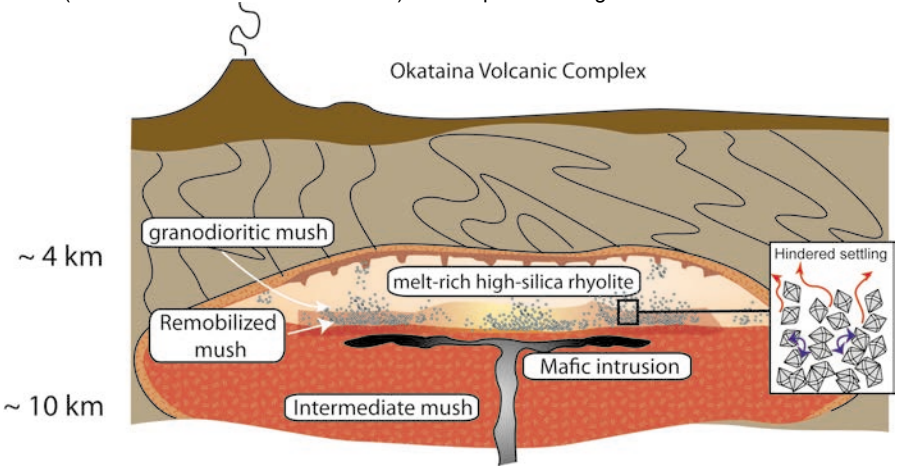
Okataina Volcanic Complex
granodioritic mush
~ 4 km
melt-rich high-silica rhyolite
Hindered settling
Remobilized mush
Mafic intrusion
~ 10 km
Intermediate mush

Table 1. Summary of orientation results.

Total grain pairs	187	
Total clusters	82	
	Number	**Percentage of total**
Pairs in Esterel or parallel orientation	114	61%
Pairs in parallel orientation	64	34%
Pairs in Esterel orientation	50	27%
Clusters with at least one pair in Esterel or parallel orientation	64	78%